The Thesis Committee for Luc Amram Lisi
Certifies that this is the approved version of the following Thesis

Using Machine Learning to Measure Ultrahigh-Flux Multi-MeV Gamma Rays from a Laser Accelerator

APPROVED BY
SUPERVISING COMMITTEE:

Micheal Downer, Supervisor

John Keto

Using Machine Learning to Measure Ultrahigh-Flux Multi-MeV Gamma Rays from a Laser Accelerator

by

Luc Amram Lisi

Thesis

Presented to the Faculty of the Graduate School of

The University of Texas at Austin

in Partial Fulfillment

of the Requirements

for the Degree of

Master of Arts

The University of Texas at Austin

December 2019

Abstract

Using Machine Learning to Measure Ultrahigh-Flux Multi-MeV Gamma Rays from a Laser Accelerator

Luc Amram Lisi, M.A.

The University of Texas at Austin, 2019

Supervisor: Michael Downer

In this thesis we present a novel computational method capable of measuring the energy distribution of ultrahigh-flux and high-energy photons ranging from 1-300MeV produced via a Thomson Backscatter process at the University of Texas at Austin Petawatt Laser facility. Due to the large and complex particle showers these kinds of photons produce when interacting with matter, energy measurements of these kinds of sources is notoriously difficult. In our method however, we make use of the complex particle showers these sources produce to extract information about the energy profile by interacting the photons with a compact inorganic scintillator. Then, using predictive simulations in Geant4 and regression analysis techniques, we analyze the raw scintillator response resulting from the incident photon shower, and compute the most likely photon energy spectrum with confidence intervals. In the following thesis, we will cover the methodology of this analysis as well as look at how it performs when applied to a recent experimental shot. Finally, we will compare the result to theoretical predictions in order to gauge the feasibility of this diagnostic method.

Table of Contents

INTRODUCTION

Chapter 1: Forward Thomson Scatter

Before we dive into the main topic of this thesis, first we must overview the physical process known as Thomson Backscatter which we will abbreviate as TBS. Also sometimes referred to by its analogous quantum process Compton Backscatter (CBS), Thomson Backscatter refers to a process where a large number of high-energy photons are produced through the interaction of a high intensity laser pulse and a counter propagating high energy electron beam. Because the electrons and laser pulse are counter propagating, and because of the high energy of the electrons, a relativistic Doppler factor arises. This Doppler shift can be intuitively understood as the laser pulse's wavelength "seen" in the rest frame of highly relativistic electrons. We can write this new wavelength explicitly as follows:

$$\lambda' = \frac{\lambda_0 \gamma_\perp^2}{[(1+\beta_0)\gamma_0]^2}$$

Where λ' represents the Doppler shifted wavelength, λ_0 represents the initial laser wavelength, and $\gamma_0 = (1-\beta_0^2)^{-\frac{1}{2}}$ where $\beta_0 = v_0/c$. In the expression for β_0, v_0 is the velocity of the electrons in the lab frame. Finally, $\gamma_\perp^2$ is a parameter defined as:

$$\gamma_\perp^2 = 1 + \frac{a_0}{2}.$$

As is the case for classical Thomson scattering, when this electron interacts with this new radiation field, it will radiate away photons at that wavelength (referred to as the fundamental) as well as at shorter wavelengths due to higher order, non-linear effects [1].

For radiation of the fundamental, we can succinctly obtain an equation for the backscattered photon energy (E_p), as a function of electron energy (E_b), laser wavelength (λ), and a laser intensity parameter (a_0):

$$E_p\,[keV] \;=\; \frac{0.019\;E_b^2[MeV]}{\left(1+\frac{a_0^2}{2}\right)\lambda[\mu m]}$$

It should be noted here that in this notation, the units in square brackets represents the units for the previous variable. Further, a_0, our unitless laser parameter, can be expressed as follows:

$$a_0 = 0.85 \times 10^{-9}\lambda_0[\mu m]I_0^{1/2}[\frac{W}{cm^2}]$$

Where λ_0 represents the incident laser wavelength and I_0 is the incident laser intensity given in watts per centimeter squared. [1]

NONLINEAR TBS:

Thomson radiation at the fundamental, as described above, is not the entire picture however. We also should take the time to note that as laser intensity increases, higher order modes of the fundamental will be seen due to higher order nonlinear terms in the laser-electron interaction becoming significant. We will differentiate this regime where higher order modes begin to have strong effect as "nonlinear TBS", as compared to "linear TBS" where the fundamental dominates. The entire derivation of the full radiation spectrum in the nonlinear TBS regime is unfortunately excluded from this thesis for the sake of brevity. However, we will quickly outline some of the important points below as the entire analytic expression for the radiated photon spectra is used in theoretical calculations of the TBS spectra later in this thesis.

First, we note that in the limit that $a_0 << 1$, linear TBS dominates, and we can consider the radiation generated by TBS to be almost entirely given by the above equations. However, as $a_0 > 1$ many higher order modes begin to appear. Eventually, we can begin to approximate the higher harmonics generated to be a nearly continuous spectrum extending out to some critical harmonic number, n_c, given by $n_c \approx \frac{3a_0^2}{4}$. An detailed discussion of an analytic approximation for the intensity spectrum with respect to radiated frequency can be found in the paper titled *Nonlinear Tomson scattering of intense laser pulses from beams and plasmas* by E. Esarey *et. Al.* Phys Rev E 1993 [1]

THE TEXAS PETAWATT LASER:

Thanks to the invention of ultra-short, femtosecond lasers and the development of chirped-pulse amplification [2], both the generation of the high energy electrons *and* the

generation of short laser pulses with intensities required for both linear and nonlinear TBS is reasonably obtainable in a single compact system. [3]

Here at the University of Texas at Austin, we are home to a state-of-the-art petawatt class laser system capable of delivering up to 150 Joules of energy on target at a pulse length of 150 femtoseconds (fs) at a repetition rate of ~1 shot/hour. However, it should be noted that more often, the facility operates in the <120J with a pulse duration of approximately 140-150fs. In order to achieve these energies and pulse durations, the Texas Petawatt Facility (TPW) uses optical parametric chirped pulse amplification (OPCPA) and a mixed glass Nd:glass amplifier [4]. For context, a brief schematic overview of the TPW OPCPA/Nd:glass system is outlined below for reference.

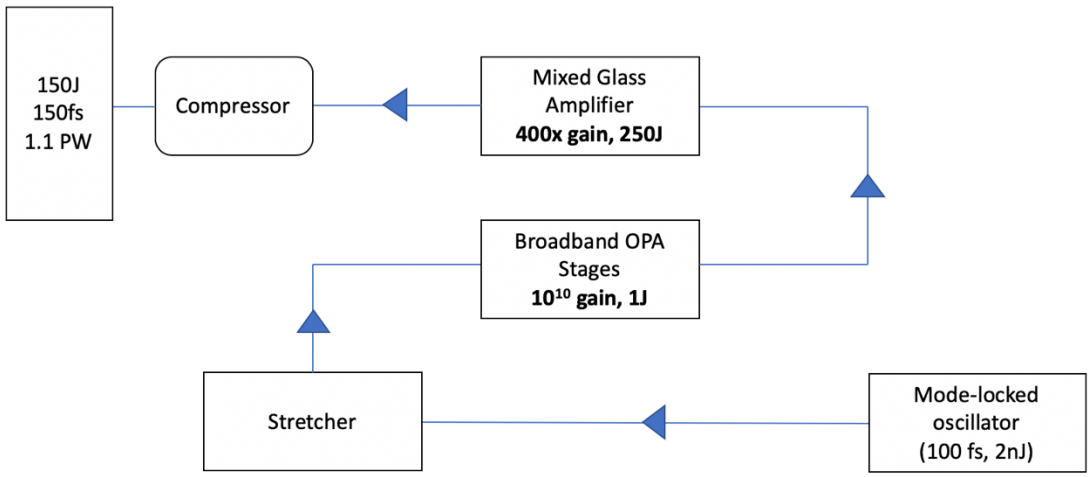

Figure 1: Texas Petawatt Laser Schematic

Above, we see a rough outline of the Texas Petawatt laser chain which includes a mode-locked oscillator operating at 2nJ and 100fs, a stretcher to separate the broadband laser pulse in time, a multi-stage optical parametric amplifier capable of a 10^{10} gain factor, a mixed glass amplifier capable of a ~400x gain factor, and finally a compressor which

simply reverses the temporal stretching of the initial gratings. [4] The final pulse can then be focused with either an f/40 spherical mirror, f/4 off-axis parabola (OAP), or an f/1 OAP. For the experiment outlined in this thesis, the f/40 spherical mirror is used.

ELECTRON GENERATION

Once this laser pulse has been obtained, we of course want to use it! Remember the high energy electron beam we wanted for TBS? Using this compressed, high energy laser pulse we can produce high energy electrons using a process known as Laser Wakefield Acceleration (LWFA). LWFA is a process where a high intensity electromagnetic field can drive waves of charge inside of plasma which, as a result of the pondermotive force, transfers energy to the surrounding electrons.[5] When these plasma waves become large enough, these electrons can become "trapped" in the propagating charge gradient and get accelerated to very high energies over very short distances. At the petawatt, we can regularly accelerate electron bunches to 2 GeV with sub-milliradian divergence. [6]

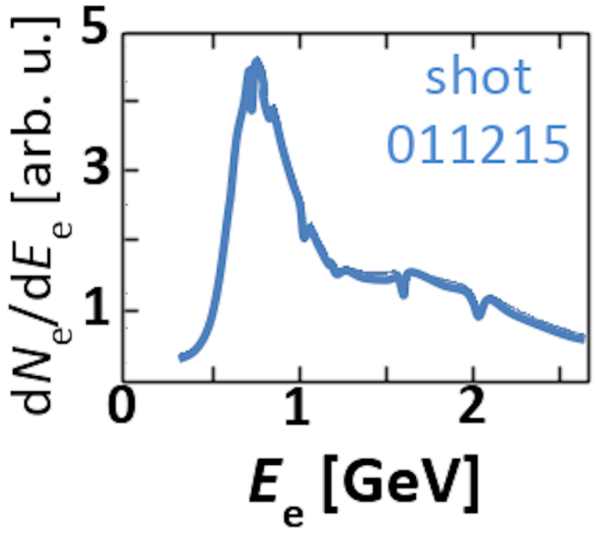

Figure 2: Example LWFA Electron Energy Distribution

Above, we provide an example of a measured electron spectrum in a recent experiment. As we can see, energies up to 2 GeV and greater can be achieved using LWFA at the Texas Petawatt.

BACKSCATTER

Now that we have the electrons, the last component needed to produce our TBS photons is a counter propagating laser pulse. By the nature of LWFA, the electrons that we accelerate will *be co-propagating* with the laser pulse. However, by using a mirror at the exit of the gas cell, the location where laser-wakefield acceleration occurs, we can simply reflect the laser pulse backwards onto the slightly slower electron bunch. To do this, we use a special kind of mirror known as a plasma mirror which is quite simply a piece of glass or plastic of small thickness. As the intense laser pulse heats the material, the material undergoes a rapid transition to a plasma state which changes its properties from almost entirely transmittive, to nearly 100% reflective. [7]. Once reflected, the now counter-propagating laser pulse will interact with our high energy electron beam in the way we hoped producing TBS.

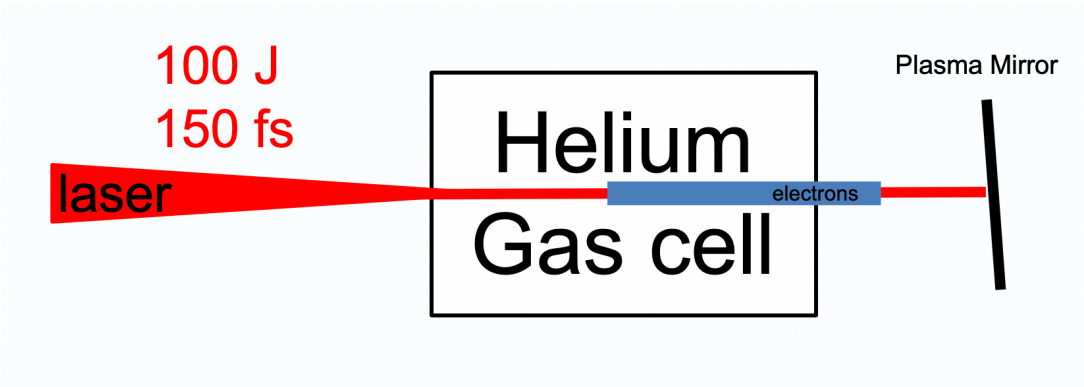

Figure 3: Thomson Backscatter Generation Schematic

Chapter 2: Particle Matter Interactions

Now that we have overviewed the process by which the Thomson Backscatter photons are created in this experiment, it is critical we take a moment to understand how these photons will interact with matter. Afterall, the topic of this thesis is how we can measure these high energy photons and to do that, we need to understand particle dynamics, and particle detectors.

PHOTON INTERACTIONS

When a photon interacts with matter, it can lose energy in multiple different ways. At low energy, these possible interaction modes are generally dominated by the photoelectric effect [8] and to a lesser extent, Raleigh scattering and photonuclear absorption. [9] Further, at low energies the cross section of these processes is very large and dominates over essentially all other processes. As a result, low energy photons cannot generally penetrate very deep into a dense solid material unless it has special optical properties that allow for it. However, at higher energies (keV and greater) the cross section for the above processes rapidly decrease and processes such as Compton Scattering [7] and pair production become much more likely. In this regime, rather than simply losing energy gradually to ionizing radiation effects, the photon can give large amounts of energy to other particles such as electrons in Compton scattering, or by completely changing forms as is the case in pair production where the photon becomes a positron-electron pair.

The cross sections for all of these interactions can be measured or calculated and is normally expressed in a tabular form with respect to the current photon energy. In the case of only a single scattering event, the probability of interaction can be calculated relatively simply using the following formula:

$$P = 1 - e^{-t/\lambda}$$

Here, t is the thickness of the material, and λ is the mean free path of the interaction.

However, in reality the photon will scatter multiple times over its entire journey in a material. In the low energy regime this is not a large issue as we can model the energy loss of a photon with respect to distance traveled in a material as a smooth and continuous function. In the high energy case however, one can see that the problem becomes analytically impossible. This is because the photon can spontaneously excite electrons to very high energies or undergo pair production which will create an entirely new set of particles. These particles then will themselves undergo the same processes in turn producing even more particles and soon, an entire ensemble of high energy particles are propagating through our material all with their own probabilistic trajectories. This is known in particle physics as a "particle shower" and we turn to computer software in order to simulate these dynamics accurately.

GEANT4 SIMULATION TOOLKIT:

In this thesis, we will make use of a particle simulation toolkit known as Geant4 to predict the showering characteristics of the TBS photons. Geant4 is able to track the passage of particles through matter from low eV-scale energies, up to TeV scale energies and larger. [10] It does this by using a Monte Carlo simulation method which determines a particle's showering behavior by continuously sampling from an underlying probability distributions. In this case, the underlying probability distributions are the cross-sections of all the possible interactions for the particle at every time step. These interactions can include both spontaneous interactions, such as the spontaneous decay of a pion, or a "stimulated" interaction such as pair production of a photon in a high Z material.

Developed at CERN specifically for particle-matter interaction simulations, Geant4 has been repeatedly tested and validated by experiments around the globe including ATLAS, CMS, BaBar, and many others. [11][12] It is capable of simulating both quantum electrodynamic (QED) interactions as well as quantum chromodynamic (QCD) interactions and can even be modified to include beyond the standard model processes such as supersymmetric particle decay.

In this experiment, we make use of the FTFP_BERT physics list and the G4EmPenelopePhysics physics list [13][14] to properly capture not only the high energy electromagnetic and hadronic processes that may occur, but also to maintain a high accuracy of lower energy (sub MeV) electromagnetic processes.

SCINTILLATING DETECTORS

In the final section of this chapter, we will briefly discuss scintillation-based detectors, or scintillators for short, as they play an integral role in this experiment. Put simply, a scintillator is a special type of material that luminesces when the material absorbs energy, generally in the form of ionizing radiation. Generally, these materials are inorganic crystals such as CsI or NaI, but they can also be formed out of organic crystals such as anthracene ($C_{14}H_{10}$) [15]. As the ionizing radiation deposits energy in the crystal structure, the underlying atomic structure will become excited and as the state relaxes, it emits an optical photon. In general, the number of photons emitted from a scintillator is assumed to be linearly proportional to the amount of energy deposited in a scintillator as long as the incident particle has sufficiently low mass compared to that of a proton. [15] As a result, for our experiment, which deals almost exclusively with electrons and photons, we will assume this linearity holds.

As a detector, scintillators have been used in a large number of different applications including old CRT monitors, and photon multiplier tubes (PMTs). Most relevant to our experiment, however, is the usage of scintillators as particle detectors. In the following chapters, we will discuss how we can make use of an inorganic LYSO(Ce) scintillator to detect characteristic features of a photon shower and how we can use these characteristic features to estimate the incident photon spectrum.

Chapter 3: Motivation

Finally, before we go into the details of the experiment that will make up the final portion of this thesis, let us briefly describe the motivation for this kind of research.

It is well known that Laser wakefield accelerators are able to provide a compact source of ultrashort-pulsed x-rays ranging from broadband keV betatron emission [16] to narrower band MeV Thomson backscatter (TBS) centered at energy:

$$E_\gamma = 4\gamma^2 h\nu$$

As described in Chapter 1, γ = accelerated electron's Lorentz factor, $h = 4.135 \times 10^{-35}$ eV s, and ν = incident laser frequency.

Previously, TBS generation up to $E_\gamma \approx 30$ MeV from LWFA electrons with $\gamma \approx 1000$ has been reported [17] and more recently, our group reported $E_\gamma \approx 100$ MeV from $\gamma \approx$ 4000 LWFA electrons [3]. In the low energy regime, methods such as K-edge filters can be implemented in order to try and measure the photon energies, but as we grow into the multi-MeV range, TBS gamma-ray measurement becomes particularly difficult. This is primarily due to the very large number of secondary particles produced during their interaction with matter as the cross-section for pair production begins to dominate (See Chapter 2). Recent efforts have been made to design gamma-ray conversion spectrometers which show promise in the 1-40 MeV range, but generally can sufferer from poor accuracy with photon energies exceedingly roughly 50 MeV. [18][19] As laser systems become capable of producing higher energy electron beams, and higher intensity lasers the need for a reliable diagnostic able to measure these higher energy gamma rays becomes critical.

In the remainder of this thesis, we will outline a novel scintillator-based method for the measurement of a high flux photon energy spectra ranging from 1-300 MeV in a single-shot setting. This method will use Geant4 to simulate particle dynamics and adopts a least-squares regression model to obtain a maximum likelihood estimation for the on-shot TBS energy spectrum based on scintillator response characteristics. In addition to this, as we will see this method is inexpensive and easy to implement using minimal computing power and experimental resources.

EXPERIMENT

Chapter 4: Experimental Setup

In order to generate these multi-MeV gamma rays, we implement a TBS setup as described in Chapter 1. As outlined in the figure below, we focus the compressed beam from the Texas Petawatt Laser into a helium gas cell with an f/40 spherical mirror. During this process, the laser pulse drives laser wakefield acceleration and accelerates our electrons up to 2 GeV in energy. As the laser pulse exits the gas cell, it is reflected at near normal incidence back towards the now counter-propagating wakefield electron bunch and upon collision, a high energy Thomson Backscatter is produced. After this scatter, the LWFA electrons are deflected from their original straight path via a magnetic spectrometer which measures the energy of our LWFA electrons (Figure 2). The uncharged gamma rays however, unaffected by the magnetic field, continue to propagate for 2-meters where they pass through a 12-inch long, 2-inch diameter lead collimator. Because of the incredibly low divergence expected from TBS, the TBS photons will be completely unaffected by this additional material. However, larger divergence background, such as bremsstrahlung, will be largely filtered out. After this collimator, the photons continue to propagate another 2-meters where they encounter a thin piece of carbon, used for a separate pair-producing spectrometer diagnostic. It should be noted here that the thickness of the carbon used in this separate diagnostic was negligibly small is not expected to have affected our final diagnostic in any way. Finally, at the end of this line lies our LYSO(Ce) scintillating detector.

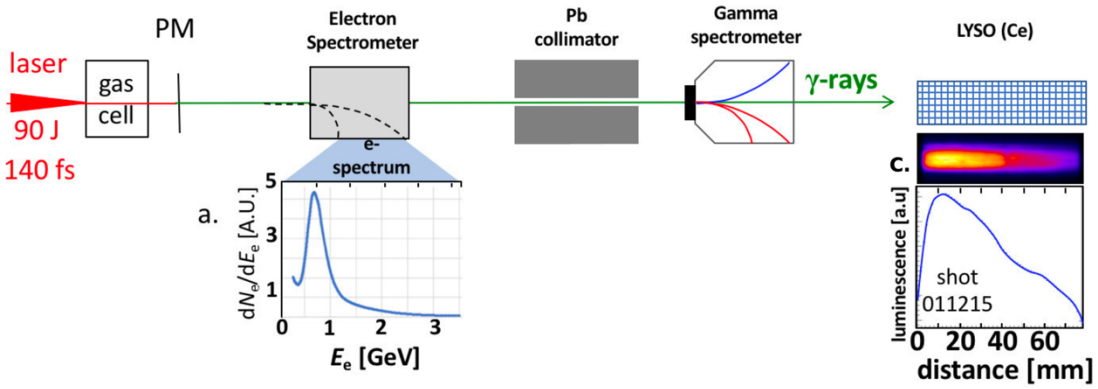

Figure 4: Full Experimental Schematic.

Note: The gamma spectrometer diagnostic will not be discussed in detail in this thesis.

LYSO(CE) DETECTOR:

The scintillating diagnostic used in this experiment was a lutetium-yttrium oxyorthosilicate, cerium doped (LYSO(Ce)) inorganic scintillating crystal. The scintillator is of dimensions 78mm x 65 mm x 12 mm and pixilated with 1.2 mm x 1.2 mm x 12 mm pixels. All but one side of the pixels were treated with a reflective coating ($BaSO_4$), and the scintillator was oriented such that the open face of the pixels was orthogonal to the incoming TBS beam. With this orientation, we aimed to capture an image of the transverse showering profile of the high energy photons by looking at the scintillating photons emitted from the open end of our pixilated detector. Because LYSO(Ce) scintillators radiate in the 450nm range, a 14 bit PCO ultraviolet charge-coupled device (CCD) camera and a simple imaging setup was used to readout the signal.

LYSO was chosen in this case due to its relatively high density (7.1 g/cm^3) in addition to its high light yield of 33200 photons/MeV [20]. Because of these features, only

a fairly small scintillator was needed in order to provide adequate stopping power for photons up to 300 MeV. However, it should be noted that one could easily use any other scintillating material in place of LYSO and the choice of LYSO was merely one of material convenience.

Upon interaction of photons with this detector, we obtain a raw detector readout from the CCD camera.

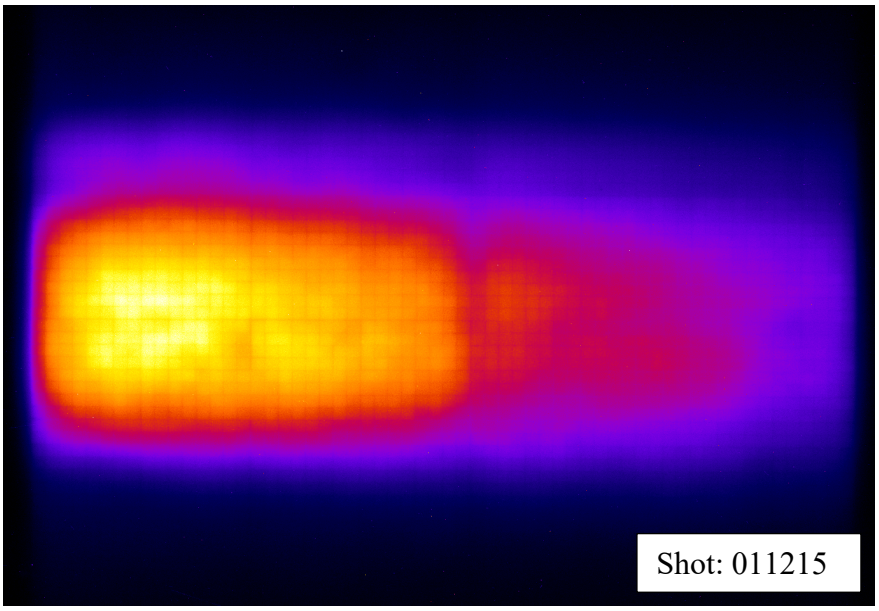

Figure 5: On-shot False Color Image of Scintillator Signal (Shot 11215)

In this image, the TBS photons are entering from the left, and we can see the scintillator response due to the evolving shower as they penetrate deeper into the material. We can also see the distinct pixelated structure of the scintillator. A few important features to note here is how the signal increases as we enter deeper into the crystal (left to right) until it reaches some peak, after which it falls off. It is this transverse profile feature of the

showering photons that we wish to use to extract information about our photon energy spectrum incident on our detector. Integrating vertically along the signal shown in Figure 5, we obtain this what we will refer to as the transverse showering profile:

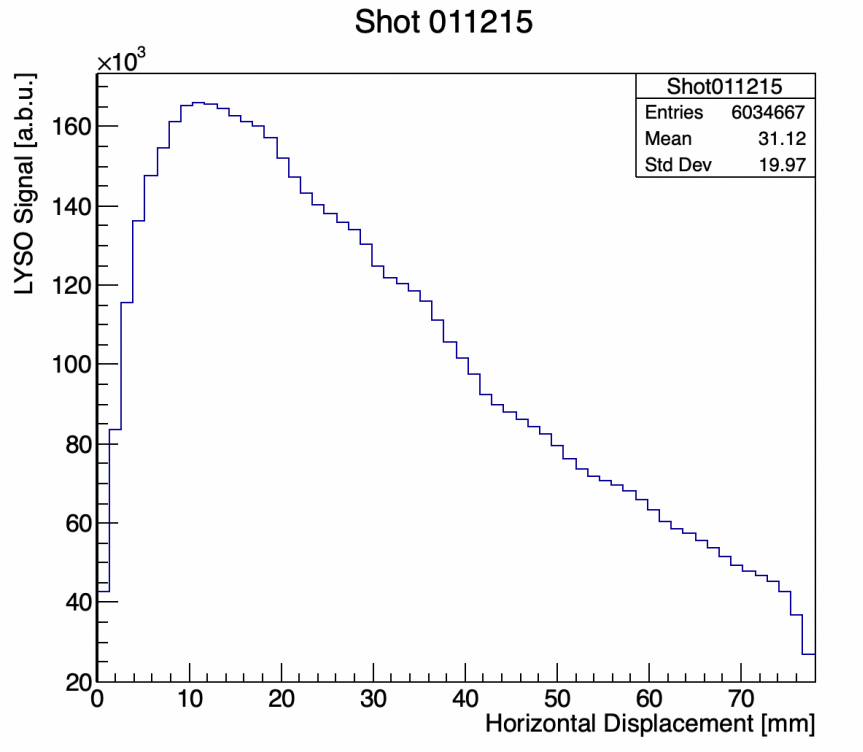

Figure 6: The Transverse Showering Profile (Shot 11215)

To calculate this, we use ImageJ [21] to obtain a vertically integrated lineout of our CCD readout (Figure 4). We also perform a Fourier filter on the scintillator image in order to remove noise that would be introduced from the small 0.1 mm thick reflective material in-between each pixel.

SIGNAL SIMULATION IN GEANT4:

Because our main observable in this detector is the transverse showering profile, it is important we understand how this feature is affected by our signal. In order to understand how this transverse showing profile depends on photon energy, we turn to Geant4. In Geant4, we model our LYSO(Ce) detector with full geometry so that it has the exact same dimensions, materials, and properties of our physical detector. Below is a rendered image of our simulated scintillator that we will use in subsequent analysis.

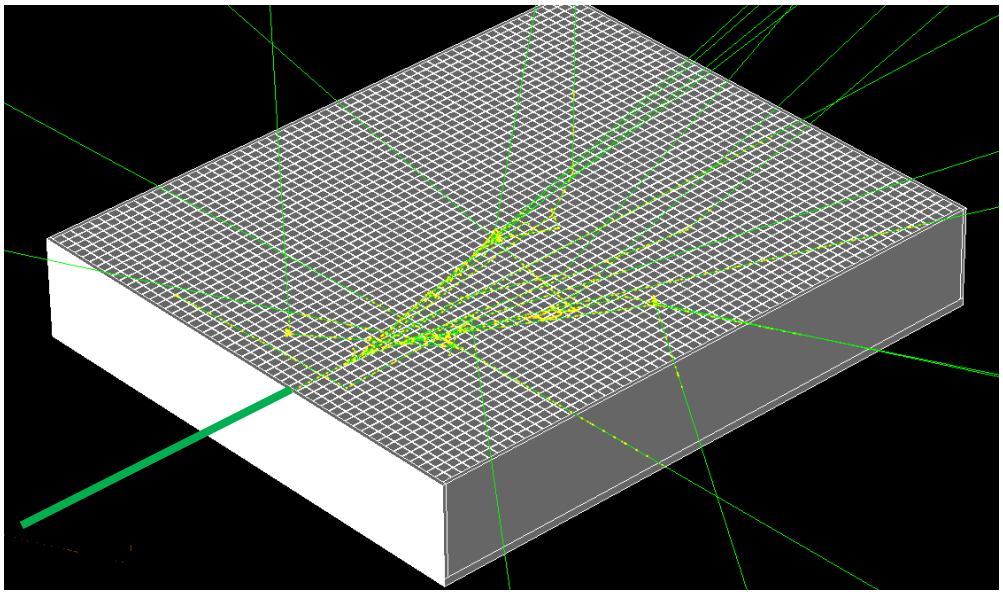

Figure 7: Full Geometry LYSO(Ce) Scintillator in Geant4 with Example Shower

In this image, we also create an example shower from a single 100 MeV photon entering from the bottom left of the image (green line given added thickness for clarity). As the photon enters, it pair produces and scatters many times and produces multiple secondary photons, electrons, and positrons denoted by the thin green lines. The yellow dots indicate a point of scattering. This is added to show how complicated even the shower

of a *single photon* can be in this detector and emphasize the need for predictive particle-matter simulation packages like Geant4.

Now, our goal here is to take a transverse showering profile, like in Figure 5, and extract the photon energy spectrum that created it. To do this, we must understand how the transverse showering profile depends on photon energy and so, we turn to Geant4. In Geant4, we propagate a series of different mono-energetic photon beams into our simulated scintillator geometry. For each mono-energetic photon beam, we obtain a simulated "readout" of our detector, and treat the simulated data just as we would real data from our experiment. Below, we show two different mono-energetic photon beams of 10 MeV and 40 MeV respectively. It should be noted that for all of these simulations, we use a beam of 10^6 photons to produce a result with sufficient statistics. Further, we assume a gaussian spatial profile of the beam of $\mu = 8.2$mm. However, we can show that the transverse showing profile is, in fact, agnostic to the spatial profile of the TBS beam provided the beam is able to fit within the scintillator. This is because while the vertical axis will have higher variance, the photons do not interact with one another and as a result, the total vertical sum of the signal will be unchanged.

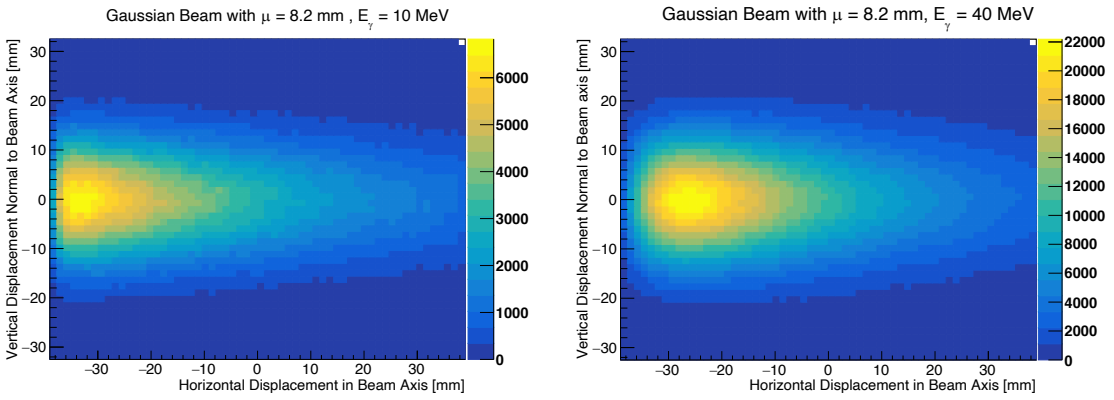

Figure 8: Simulated LYSO Signal

Here we see two different simulated signals both with the same number of incident photons but different photon energies, 10MeV and 40 MeV on the left and right respectively. Note how the 2D transverse showering profile changes as the energy increases. As we start simulating many different photon energies, we are able to provide a picture of how the shower profile evolves with photon energy. In this plot below, we integrate vertically across the scintillator, just like we do with the experimental signal, so that we only have scintillator signal as a function of depth. As described above, this also gives the added benefit of allowing us to ignore any uncertainly we may have in the actual TBS spatial profile.

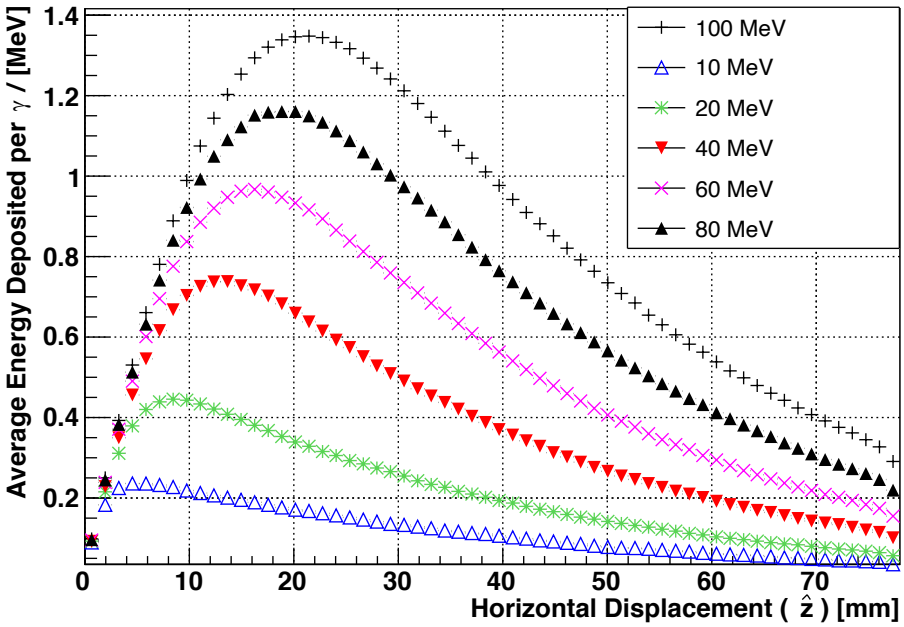

Figure 9: Transverse Showering Profile for a selection of Photon Energies

Just as we might have expected after examining Figure 8 previously, Figure 9 shows us that as the energy of our photons increase, the peak of the horizontal showering

profile pushes deeper into the scintillator and the shape changes slightly. Further, the total signal increases! Both of these features can be explained by the understanding that a higher energy photon will produce higher energy secondaries (photons, electrons, and positrons) which will 1) take longer to stop and 2) deposit more energy in the scintillator in turn produce more signal in a scintillator. In the end, we simulate these transverse showering profiles for a large array of energies ranging from sub-MeV levels (500 keV), out to 300 MeV.

USING SIMULATIONS TO PREDICT EXPERIMENTAL SIGNAL

Now that we have a large number of simulated transverse showing profiles for mono-energetic photons in our LYSO(Ce) scintillator, we make the claim that we can use the simulated showering profiles we created to produce a simulated signal from *an arbitrary energy distribution* in the range 1-300MeV with a simple linear combination of these mono-energetic signals. For example, we claim we can approximate the transverse showering profile of a signal whose distribution was 1/3 10MeV photons and 2/3 20 MeV photons as just the weighted sum of the respective mono-energetic showering profiles shown in Figure 8. We believe this to be a fair assumption based on three assumptions:

1) Photons at these energies will not interact or interfere with one another as the cross-section for photon-photon scattering is so low that, in fact, it has never even been experimentally measured.

2) Charged secondaries will also not have meaningful interactions with each other at these energies. We argue this is fair because first, the density of secondaries will still be much lower than the density solid density of atomic electrons and nucli in the solid. For example, a gamma beam of 10^9 with 1-inch diameter would produce roughly 10^{11} secondaries/cm^3.

(1000 particles per gamma) and the solid density of electrons for LYSO will be roughly 10^{23}. As a result of this 10+ order of magnitude difference, we assume the vast majority of secondary interactions will be with the scintillator. However, it might also be important to consider space-charge effects. We argue that due to the fact that at these energies we expect a uniformly even number of electrons and positions distributed across the shower, the net charge density should remain roughly neutral and not greatly affect the shape of the shower. In a future iteration, these space-charge effects could be possibly modeled much more explicitly, but for now we will hold this assumption through this thesis.

3) Finally, our last assumption is that rather than needing to simulate an infinite, continuous number of monoenergetic profiles, which seems rather impractical, we can choose a spacing such that the transverse signal of some E_i energy, is close to the result of averaging the signal from E_{i+1} and E_{i-1}. As a result, as we iterate through the simulated energies E_i , the transverse showering profile changes slowly and smoothly and any intermediate profile of some unstimulated energy E_j can be approximated as a properly weighted average of the two profiles of $E_i < E_j < E_{i+1}$.

More rigorously, we can write the previous two claims as follows:

$$S(d) = \int_0^{\infty} a(E)T(E,d)dE \approx \sum_{i=1}^{iMax} a_i\, T(E_i,d)\,(E_i - E_{i-1})$$

$$T(E_j,d) \approx \frac{a_i T(E_i,d) + a_{i+1}T(E_{i+1},d)}{2} \quad , \quad E_i < E_j < E_{i+1}$$

Here, $a(E)$ is the true continuous photon energy distribution and $T(E,d)$ represents the transverse showering profile at some incident photon energy E. By or first

claim, this integral, $S(d)$, is then just the total transverse showering profile which is only a function of horizontal depth d in our detector. However, because a continuous and infinite number of monoenergetic signals cannot be simulated, we approximate this as a Reimann sum with discretely sampled E_i's such that the second condition is met. In this second statement, E_i and E_{i+1} represent some simulated energies and E_j represents some arbitrary unstimulated energy between them. The spacing of $(E_i - E_{i-1})$ is chosen such that this condition is met. Essentially, this is a statement that our discrete samples form a basis that spans the space of possible profiles between some E_{min} and E_{max}.

FITTING SIGNAL USING LEAST SQUARES AND SIMULATED ANNEALING

Now that we have argued that our signal S(d) can be approximated by the discrete sum of transverse energy profiles, we simply need to find a set of weights A = $\{a_1, a_2 \dots a_n\}$ such our calculated signal $S'(d)$ best fits some real $S(d)$ that we measure on shot. To do this, we will adopt a least squares regression approach.

Least squares is a method in which one can approximate the solution highly overdetermined system by trying to minimize the sum of the squares of the residuals. In the case of fitting, this just means we want to minimize the square of the difference between our real measured signal, which I will denote $S(d)$, and our predicted signal, $S'(d, A)$, at every point along d. In other words, we wish to find some set of weights A such that we minimize $\sum(S(d_i) - S'(d_i, A))^2$.

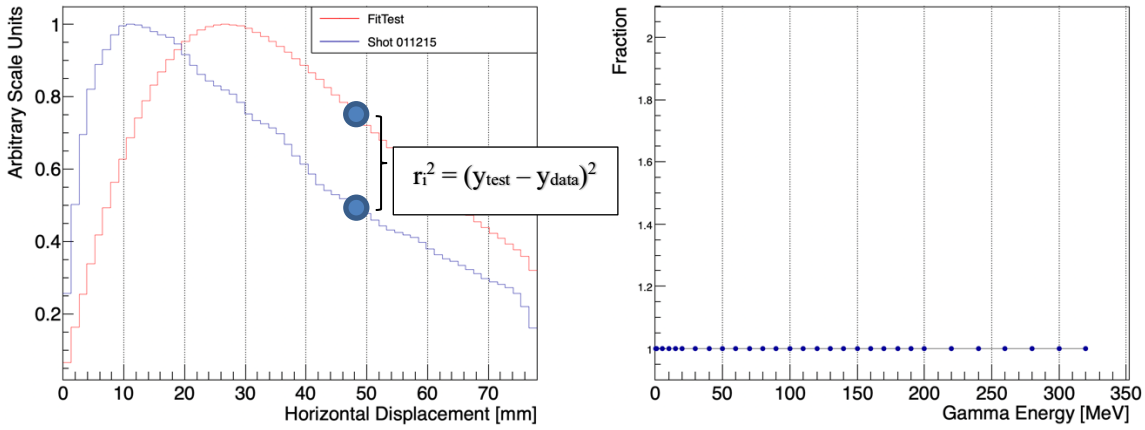

Figure 10: Fit Test with Initial Weights set to A = {1,1,1…..1}

Above on the left, we show an example of our signal $S(d)$ (in blue) and our simulated signal $S'(d, A)$ (in red). On the right, we show the value of the weights A. In this case, our weights are initialized such that all weights simply start at 1. Once properly fit, these weights can be interpreted as a predicted photon energy distribution. At no point however do we seed these initial weights with any information about the expected photon spectrum and no constraints are placed on the weights other than that they must be positive value. The goal is for this method to be entirely blind to the physics regarding how these photon were generated allowing it to be feasible to measure photon energies from completely unknown sources.

So, our goal now is to find the best set of weights A, such that we minimize the sum of residuals created a simulated signal that most closely resembles our data. To do this, we use a minimization scheme known as simulated annealing.

Simulated annealing (SA) is a computational technique used to find the global maximum or minimum of some arbitrary function.[22] Unlike other minima/maxima finding techniques such as gradient decent [23] however, SA takes a probabilistic approach which performs much better in a space where there may be many different local minima/maxima. The algorithm can be described in the following steps:

1) The system begins in some state, 's', represented by a value function F(A) where A is a set of some initialized parameters (in this case our weights) which we will need to change in order to minimize F. For us, F is the sum of squares.
2) The fitting simulation is given some initial fitting parameter T, and some initial step-size dS. Due to the name of this fitting procedure, this parameter T is sometimes referred to as the temperature in order to draw an analogy to the physical process of annealing. However, it is not to be confused with a physical temperature of our system.
3) At each time step, the system considers some neighboring state, s*, a step size dS away, and computes the new value (the sum of residuals, r) of the new state given this step represented by F(A*).
4) If the r value (sum of residuals) of the state F(A*) is lower, the system takes a step in that direction just like in gradient decent. If the value of the state is larger however, unlike gradient decent we *still* have a probability of taking a step based on the parameter T of the system. This probability is generally written as follows:

$$P = 1 \quad if \ \Delta r < 0$$

$$P = e^{-(\Delta r)/T} \ if \ \Delta r > 0$$

Here, Δr is the difference in the sum of residuals between the current state, vs the next state and T is our fitting parameter.

5) Finally, whether a step is taken or not, the parameter T is decreased, as well the step size ds.
6) The system then repeats steps 3-4 where each time the parameter T and the step size of the system continually decreases. Once we reach zero "temperature" (T = 0), or after a certain number of iterations complete, the annealing is terminated, and we return the final state's parameters A_{final}.

The benefit here is that unlike gradient decent, this kind of algorithm *can* still take steps that will kick the system out of a local minimum, especially early on when the "temperature" (T) is high. However, as the simulation continues to run, it eventually starts to mimic a "greedy" algorithm such as gradient decent, as the probability of taking a step that isn't optimal decreases exponentially with T. This "cooling" is why we refer to it as a simulated annealing.

RESULTS AND CONCLUSION

Chapter 5: Results

With all of this understood, we implement this full method to try and fit experimental data obtained during experiment. We use Python's SciPy library [24], and we take advantage of a built-in annealing function that exists in the *optimize* module and use it to attempt to optimize the initialized weights as shown in Figure 10. We ran this simulated annealing process 1000 times to account for variations in the final state obtained by our annealing, and below we present the average predicted results for our set of optimized weights A*.

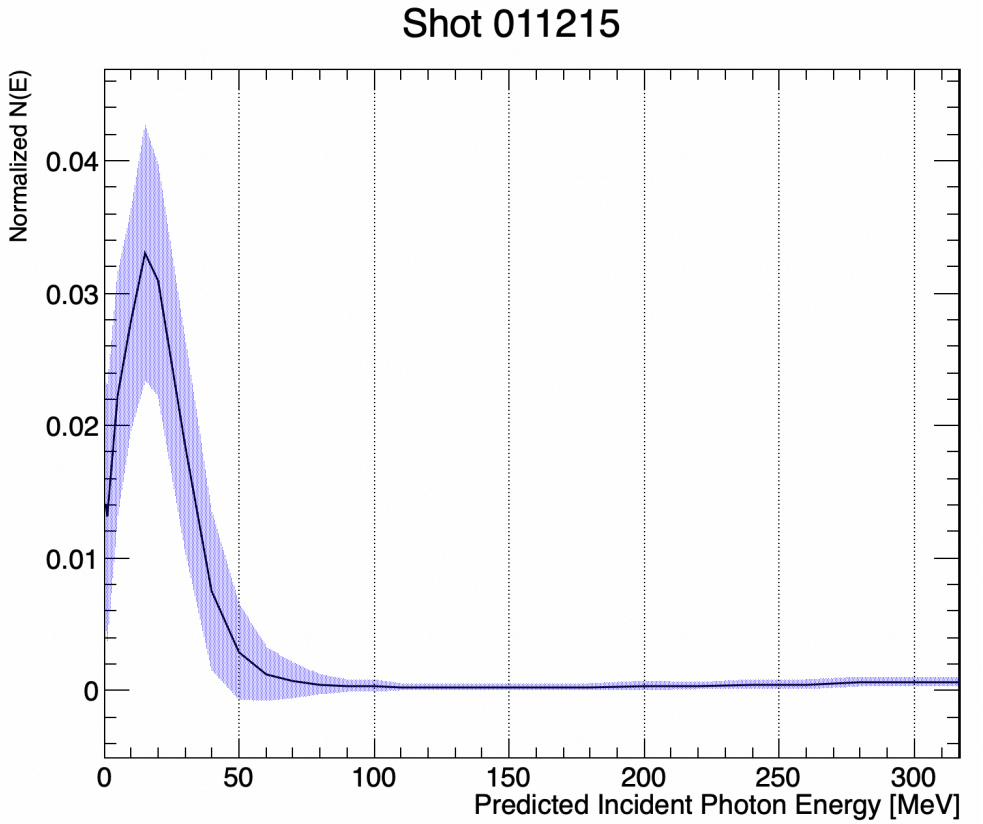

Figure 11: Best Fit Photon Energy Spectrum (Shot 011215)

Shown above is the best fit photon energy spectrum for shot 011215 during our experiment. In dark blue, we see the average value for the fraction of photons at each energy bin in x. Surrounding the line, we also include our 1-sigma confidence interval that we calculate through repeated iterations of simulated annealing.

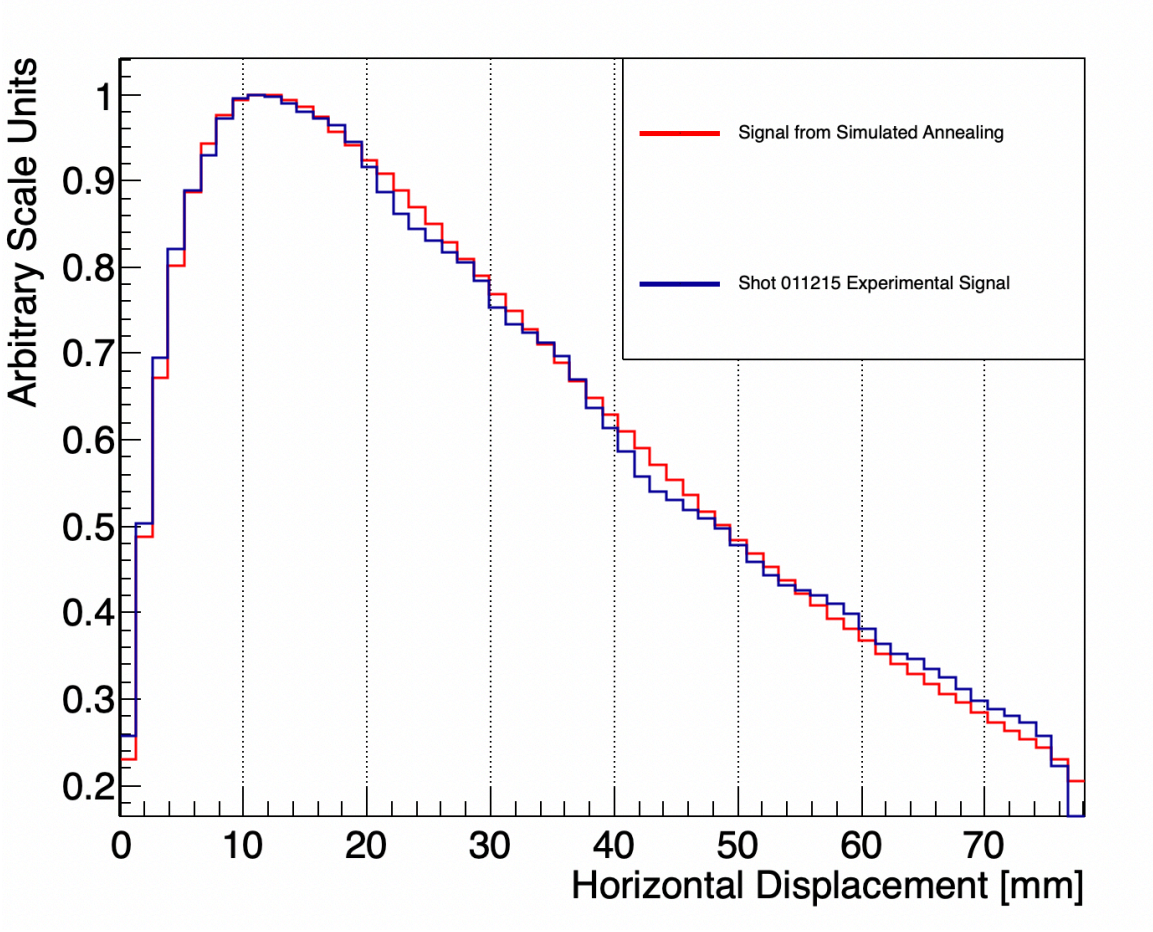

Figure 12: Goodness of Fit Comparison (Shot 011215)

Comparing the signal generated by our best fit photon spectrum using least squares and simulated annealing (red) to the signal seen in experiment (blue), we can see that it matches very well, and it appears the fit found through simulated annealing was successful in not only obtaining a best fit, but finding one that resembles something we should expect for a physical photon energy spectrum!

Chapter 6: Discussion and Conclusion

Using the method outlined above, we were able to compute the most likely photon spectrum incident on our scintillating detector using nothing more than a CCD camera, a scintillator, and Geant4. We can compare this result side-by-side with the theoretical TBS spectrum that can be calculated using the physics outlined in Chapter 1, the LWFA electron spectrum, and the laser parameters for the same shot and we see the following:

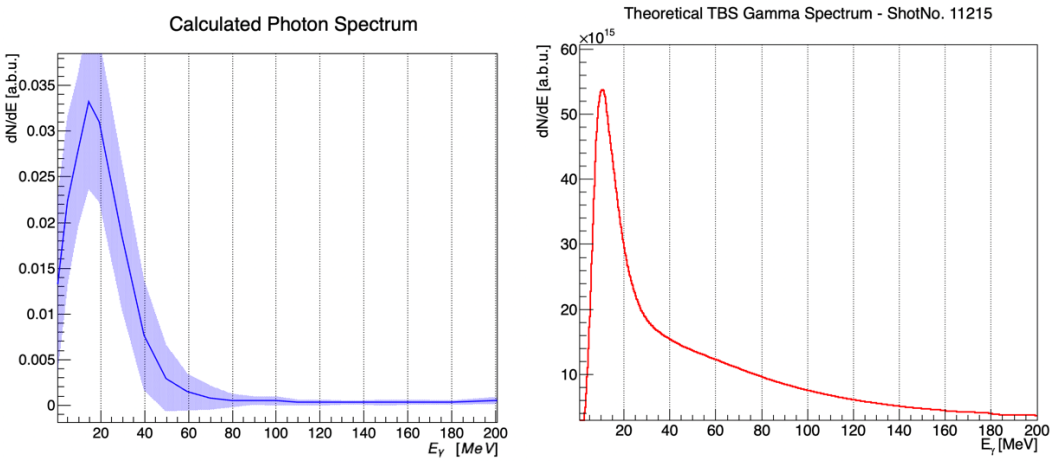

Figure 13: Calculated Photon Spectrum vs Theoretical TBS Spectrum

Qualitatively, these two results are remarkably similar. Both demonstrate a distinctive sharp peak at 10-15 MeV, something we would only find in this experiment as a result of TBS, followed by a rapid decrease in photon energy. There is some discrepancy in the 0-5 MeV range, but this can easily be explained by low energy bremsstrahlung and betatron radiation that will always be present as experimental noise. There is also another note-worthy discrepancy in the 40-80MeV range where we see our measured spectrum falls off much more rapidly than the theoretical TBS spectrum.

A possible explanation for this could be that the laser parameter (a_0) is significantly lower that what was measured. In the theoretical calculations, this would lead to a much shaper "knee" more closely resembling our calculated spectrum. However, even with these small discrepancies, it appears that we have successfully calculated a photon energy spectrum that matches theoretical predictions with no initial seeding or large statistics necessary.

In conclusion, what we present here is a low-cost, novel method of calculating the energy of high-flux, multi-MeV gamma rays in a single-shot using only a pixilated scintillator, a CCD camera, and Geant4. At no point do assumptions about the expected photon spectrum need to be made, and even though we use this method to measure TBS, this method could generalize to any high-flux, multi-MeV photon source without any modification. Computationally, this method is also very inexpensive and can be conducted on a personal laptop where analysis of a single shot takes only about 30-60 minutes-- well within the rep-rate of the TPW.

With some modification, such as automated readout and processing of the scintillator readout, one could easily field this diagnostic to measure the energy of any high-flux, high-energy photon source in a completely self-contained, turn-key system.

REFERENCES

1. E. Esarey, S. K. Ride, and P. Sprangle. “Nonlinear Thomson scattering of intense laser pulses from beams and plasmas,” Phys. Rev. E, vol. 48, pp. 3003-3021, October 1993.
2. S. Donna, et al., “Compression of amplified chirped optical pulses” Optics Com. Vol 56 pp. 219-221 1985
3. J. Shaw, et al., “Bright 5 - 85 MeV Compton gamma-ray pulses from GeV laser-plasma accelerator and plasma Mirror,” ArXiv 1705.08637, 2017.
4. E. Gaul, et. al., 2010 Appl.Opt. 49 1676 doi: 10.1364/AO.49.001676
5. T. Tajima and J.M. Dawson, Phys. Rev. Lett. 43(4) (1979) 267. http://dx.doi.org/10.1103/PhysRevLett.43.267
6. X. Wang, et al., “Quasi-monoenergetic laser-plasma acceleration of electrons to 2 GeV,” Nat. Commun., vol. 4, pp. 1988, June 2013.
7. J. D. Jackson, 1925-2016. Classical Electrodynamics. New York :Wiley, 1999.
8. Einstein, Albert(1905). "Über einen die Erzeugung und Verwandlung des Lichtes betreffenden heuristischen Gesichtspunkt" [On a Heuristic Point of View about the Creation and Conversion of Light] (PDF). *Annalen der Physik* (in German). 17 (6): 132-148.
9. Particle Data Group (pdg), “Passage of Particles Through Matter” http://pdg.lbl.gov/2019/reviews/rpp2018-rev-passage-particles-matter.pdf
10. S. Agostinelli, et al., “GEANT4: A Simulation toolkit,” Nucl. Instrum. Meth. Phys. Res., Sect. A, vol. 506, pp. 250-303, 2003.
11. J. Allison et al., Nucl. Instrum. Meth. A 835 (2016) 186-225
12. J. Allison et al., IEEE Trans. Nucl. Sci. 53 (2006) 270-278
13. Reference: Physics Lists https://geant4.web.cern.ch/node/155
14. L. Pandola et al., “Validation of the Geant4 simulation of bremsstrahlung from thick targets below 3 MeV” Nuclear Inst. and Meth. B. vol. 350, pp. 41-48
15. W, Leo, “Techniques for Nuclear and Particle Physics Experiments: A How-To Approach” 1948
16. K. Nakajima, “Toward a table-top free-electron laser,” Nature Phys. 4, 92-93 (2008)
17. J. M. Cole, et al., “Experimental evidence of radiation reaction in the collision of a high-intensity laser pulse with a laser-wakefield accelerated electron beam,” Phys. Rev. X, vol. 8, pp. 011020, February 2018.
18. D. J. Corvan, G. Sarri, and M. Zepf, “Design of a compact spectrometer for high-flux MeV gamma-ray beams,” Rev. Sci. Instrum., vol. 85, pp. 065119, 2014.
19. W. Schumaker, et al., “Measurements of high-energy radiation gener- ation from laser-wakefield accelerated electron beams,” Phys. Plasmas, vol. 21, pp. 056704, 2014.
20. https://www.crystals.saint-gobain.com/products/prelude-420-LYSO
21. https://imagej.nih.gov/ij/

22. Khachaturyan, A.; Semenovskaya, S.; Vainshtein, B. (1981). "The Thermodynamic Approach to the Structure Analysis of Crystals". Acta Crystallographica. **37** (A37): 742–754. Bibcode:1981AcCrA..37..742K. doi:10.1107/S0567739481001630.
23. S. Ruder, "An overview of gradient decent optimization algorithms" https://arxiv.org/pdf/1609.04747.pdf
24. https://www.scipy.org/
25. L. A. Lisi, et. al., Spectral Analysis of 50-100 MeV Thomson Backscatter Gamma-rays from GeV Laser-Plasma Accelerator, IEEE Advanced Accelerator Concepts Workshop Proceedings (2018)